APL Photonics

LETTER | OCTOBER 02 2025

Quantum undetected photon phase measurement on a silicon chip

Chiara Michelini ; Stefano Signorini ; Lorenzo Pavesi ; Valerio Pruneri

APL Photonics 10, 101301 (2025)
https://doi.org/10.1063/5.0282497

Quantum undetected photon phase measurement on a silicon chip

Cite as: APL Photon. 10, 101301 (2025); doi: 10.1063/5.0282497
Submitted: 26 May 2025 • Accepted: 12 September 2025 •
Published Online: 2 October 2025

View Online Export Citation CrossMark

Chiara Michelini,[1] Stefano Signorini,[2,a)] Lorenzo Pavesi,[1] and Valerio Pruneri[2,3]

AFFILIATIONS

[1] Nanoscience Laboratory, Department of Physics, University of Trento, 38123 Trento, Italy
[2] ICFO-Institut de Ciencies Fotoniques, The Barcelona Institute of Science and Technology, 08860 Castelldefels (Barcelona), Spain
[3] ICREA-Institució Catalana de Recerca i Estudis Avançats, Passeig Lluís Companys 23, 08010 Barcelona, Spain

[a)] **Author to whom correspondence should be addressed:** stefano.signorini@icfo.eu

ABSTRACT

We experimentally demonstrate undetected photon phase sensing on a silicon photonic chip. We use a novel design, implementing an innovative integrated SU(1,1) interferometer based on transverse waveguide modes, that leverages intermodal spontaneous four-wave mixing to generate highly non-degenerate idler–signal photons. In our experiment, we retrieve the phase applied to the signal photons at wavelength 1972 nm by detecting only the correlated idler photons at 1291 nm, demonstrating the first on-chip phase sensing based on undetected photons. This result paves the way for novel generations of quantum refractometric sensors.

The technological advancement in optics proceeds in lockstep with the maturity of light detection technologies. As applications are being developed exploiting high-efficiency detectors, the resulting demand for such applications drives the research on increasingly efficient, fast, and low-cost detection devices. This reinforces the development of already well-established detection technologies, especially detectors for the visible spectral region (0.38–0.75 μm)[1,2] and near-infrared (NIR) region up to the telecom wavelengths (1.26–1.68 μm).[1–3] However, measuring longer wavelengths is essential for diagnostic techniques, such as imaging[4] and gas spectroscopy.[5,6] As an example, molecules have their spectral fingerprints in the mid-infrared (MIR, 2–20 μm) region.[7] Yet, MIR detectors are heavily affected by environmental thermal noise due to the narrow energy gap that is required to detect such long wavelengths.[8] Even if cooled down to cryogenic temperatures to limit thermal noise, MIR detectors feature a lower signal-to-noise ratio than detectors sensitive to shorter wavelengths.[9] Moreover, cryogenic solutions result in expensive and bulk systems, limiting the adoption of such detection technologies, and their applications, to research laboratories.

The undetected photon (UP) technique[10] is an interferometric method that promises to solve the problem of the lack of room-temperature detectors in the MIR region. A standard design for an UP setup is the low-gain SU(1,1) configuration,[11,12] in which two identical photon-pair sources are cascaded and coherently pumped. The sources generate correlated idler and signal photons through nonlinear parametric processes. The pump intensity must be low enough to neglect the probability of simultaneous emission by both sources. The generated photon pairs from the first and second sources must be indistinguishable in all degrees of freedom, such as spectral and spatial distributions. In this way, quantum interference occurs between the two alternative events of generation in the first or in the second source. The interference pattern holds the information about the indistinguishability of the generation processes. Therefore, if a sample is placed between the two sources, the phase or absorption induced by the sample will alter the interference pattern. Due to the correlation of the photons in the pair, the signature of the interaction is carried by the whole two-photon state, and the interference pattern can be obtained by detecting only one of the two photons. If the photons in the pair are highly non-degenerate, with, for example, one photon in the MIR and the correlated one in the visible, and a sample is placed such that only the MIR photon from the first nonlinear process is going to probe it, the information about the absorption and phase due to the sample can be retrieved by looking at the visible photon only. The UP technique has been used successfully for MIR imaging[13,14] and spectroscopy.[15,16] However, these demonstrations, while removing the need for cryogenic cooling, still relied on bulk setups, with limited robustness, alignment tolerance, and portability. Integrated photonics would be the ideal technology to scale down costs and dimensions of UP systems; nevertheless, up until now, the only nonlinear circuits demonstrated on the integrated platform are limited to C-band operation.[17–19]

In this work, we report, to the best of our knowledge, the first demonstration of undetected photon phase sensing on a photonic integrated circuit (PIC). O-band photons only are detected to retrieve the phase information of the undetected correlated photons around 2 μm. The whole nonlinear interferometer, including photon pair generation and phase probing stages, is integrated on the same SOI (silicon-on-insulator) chip, resulting in significantly enhanced miniaturization and robustness compared to bulk UP systems. Moreover, since the optical modes supported by an integrated structure are spatially confined, alignment between the sources is guaranteed, maximizing their spatial indistinguishability.[20] From a broader perspective, PIC-based UP devices hold the promise of compatibility with mass-manufacturable consumer electronics, offering great potential for commercial technological applications. In particular, our design enables the development of integrated refractometric sensors[21] based on undetected photons.

To enable broadband spectral operation and stable photon manipulation, we took advantage of transverse waveguide modes to design a novel schematic for UP measurements. Our UP configuration consists of an innovative SU(1,1) interferometer embedding mode converters and intermodal spontaneous four-wave mixing (SFWM) sources.[22] The photon sources are multimode waveguides pumped using a continuous wave (CW) C-band laser. The pump is split equally on the transverse electric fundamental (TE0) and first excited (TE1) optical modes. Phase matching is met with the idler and signal photons in the TE0 and TE1 modes, respectively. Working with the transverse waveguide-mode degree of freedom gives two advantages: first, it provides access to intermodal parametric processes, characterized by perfect phase matching at largely non-degenerate wavelengths, allowing for easier spectral filtering and increased spectral tunability of the generated photons; second, it allows for efficient on-chip separation and manipulation of idler and signal photons by leveraging the transverse waveguide-mode degree of freedom. Figure 1(a) reports the measured spectral wavelengths of the idler and signal as a function of the pump wavelength, demonstrating the high non-degeneracy of the photons and the notable spectral tunability of the process. A further advantage of intermodal sources is the high inter-source spectral indistinguishability.[23] In Fig. 1(b), the idler emission spectra of two nominally identical sources are compared. These sources belong to the same chip and resulted in 99.75(6)% average spectral indistinguishability, measured with four different chips and as many pairs of sources.

The general schematic for our design is outlined in Fig. 2(a), which portraits a standard SU(1,1) interferometer.[11] Two pump beams, on the TE0 and TE1 modes and, respectively, labeled as p_0 and p_1, pump two cascaded nonlinear optical sources, generating correlated idler and signal photons (i and s) via SFWM.

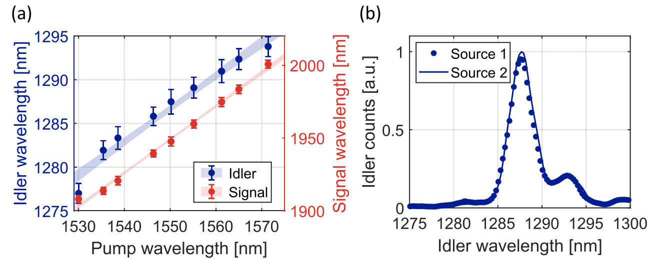

FIG. 1. Sources characterization. (a) Idler and signal central wavelengths as a function of the pump wavelength. The dots represent experimental data and the shaded color represents linear regression with its uncertainty. (b) Idler spectra of two nominally identical sources on the same chip. The pump wavelength is 1550 nm.

The pump power is kept low enough to guarantee the single-photon level operation of the sources such that the probability of simultaneous generation by both sources is negligible. Our design includes a phase manipulation stage between the sources that allows arbitrarily applying an individual phase γ_j to each of the beams ($j = p_0, p_1, i, s$). To verify that our design can successfully be used to carry out on-chip UP measurements, we operate the system by retrieving a known phase applied to the signal by only detecting the single-photon interference of the idler. It is important to stress that interference can be observed in the idler photon counts varying the phase of any photon involved in the process.[15] When a phase is applied to the signal or to the idler, it affects the whole pair generated in the first nonlinear source. If the phase is applied to the pumps, it will be carried by the photons generated in the second source. The probability amplitudes of generation in either source interfere, and the probability P_i of detecting the idler is (see Appendix A)

$$P_i = \frac{1}{2}\left[1 + \cos\left(\gamma_{p_0} + \gamma_{p_1} - \gamma_i - \gamma_s\right)\right]. \tag{1}$$

The on-chip implementation is shown in Fig. 2(b). First, the pump beams are prepared in the TE0 and TE1 optical modes. A tapered lensed fiber is edge-coupled to the chip to inject a CW laser beam, and to optimize the coupling, an on-chip inverse tapered coupler is used. The laser beam is then split on-chip with a 1 × 2 50:50 multimode interferometer (MMI). Two coherent identical beams are collected using two single-mode waveguides, one of which adiabatically broadens to a multimode waveguide. With an asymmetric directional coupler[24] (ADC), the TE0 pump beam propagating in the single-mode waveguide is coupled to the TE1 optical mode supported by the multimode waveguide.

The pumps propagate in the first nonlinear optical source, which is a 7.5 mm long multimode channel waveguide made of silicon embedded in silica, with cross section 220 nm × 2 μm. To fit such a long waveguide into a shorter chip, the source consists in three straight waveguides connected by curves.

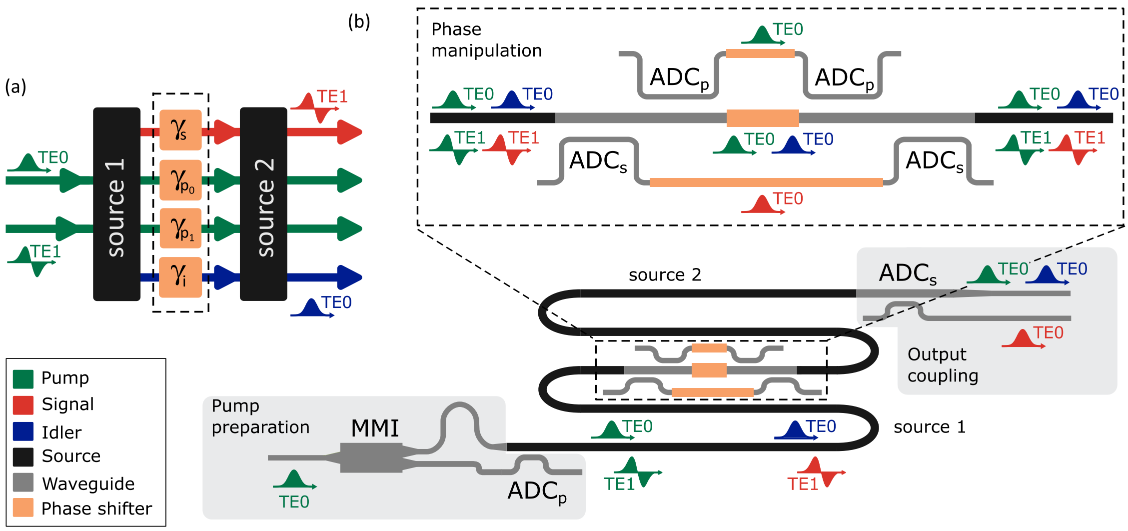

FIG. 2. Chip design. (a) Conceptual representation of the design. (b) Schematic of the integrated circuit. MMI: multimode interferometer. ADC: asymmetric directional coupler. The subscript $j = p$ ($j = s$) indicates that the ADC is designed to couple efficiently in the spectral region of the pump (signal). This scheme is not in scale.

After the first source, there is a phase manipulation stage, where the pump p_1 and the generated signal photons, i.e., the beams in the TE1 modes, are individually separated with a system of ADCs. The geometry of each ADC has been optimized for the specific wavelength involved and is detailed in Appendix B. Phases on-chip are selectively applied by using thermo-optic phase shifters.

After the phase manipulation stage, the pumps, idler, and signal are recombined and fed into the second source. In this way, we preserve the path indistinguishability of the generated photons.

Finally, at the outcoupling stage, the signal and idler are separated by means of an ADC. The multimode waveguide in which the pumps and the idler propagate tapers off to a single-mode waveguide, to radiate the TE1 pump mode in the cladding of the integrated circuit. The idler and the residual p_0 pump are outcoupled with a tapered lensed fiber. The idler photons are isolated from pump, signal, and Raman noise by cascading two fiber-based notch filters (1550 nm center wavelength, 30 nm bandwidth) and two fiber-based bandpass filters (1290 nm center wavelength, 15 nm bandwidth). More than 40 dB and 100 dB suppression is achieved for Raman and pump noise, respectively. The idler is detected using an InGaAs single-photon avalanche diode (free-running, 10% detection efficiency, 1 μs dead time), which also provides further suppression of signal photons, being sensitive up to 1700 nm wavelengths only.

The novelty of our design lies in combining photon pair sources and multiplexing strategies both based on transverse waveguide-modes as the fundamental degree-of-freedom. In traditional SU(1,1) interferometers and UP circuits, the multiplexing is based on the spectral degree-of-freedom; however, this is not efficient for PIC based implementations. Mach–Zehnder interferometers[17] or ring resonators can be used but with limited bandwidth operation, thermal stability, fabrication tolerance, and spectral tunability. Multiplexing based on transverse waveguide-modes, especially when using ADCs for mode conversion, guarantees broadband operation, thermal stability, and fabrication tolerance. In brief, our SU(1,1) interferometer combines the highly non-degenerate generation of intermodal SFWM sources with the stable and selective operation of ADCs, enabling individual manipulation of photons and on-chip separation of idler and signal, thanks to their different transverse waveguide-modes.

We initially characterized the classic behavior of the circuit by monitoring the residual pump intensity at the idler output as a function of γ_{p1} and γ_s. In this way, we measured a phase contribution on the pump as the signal phase shifter was operated, as reported in Fig. 3(a). We attribute this behavior to the spurious coupling of part of the pump p_1 to the first signal ADC (ADC$_s$). From full-3D FDTD simulations, we quantify in about 10% the coupling of the pump p_1 to ADC$_s$. When applying a phase γ_s to the signal, the part of pump leaking into the signal phase-shifting arm gets an additional phase contribution φ_p. Moreover, since the pump ADC is not 100% efficient (see Appendix B), some of the p_1 power does not couple to the pump phase-shifting arm. The p_1 beam is thus taking three different paths, as illustrated in Fig. 3(b), giving rise to a three-branch interferometer. The characterized spurious phase shift on the pump beam will be taken into account later to analyze the UP measurements. The spurious contribution will be indicated with the letter φ to discriminate it from the voluntarily induced phase shift γ.

In order to perform the UP measurements, we used a CW pump at 1561 nm, with an on-chip power of 5 mW. The pair-generated rate for an individual source is about 100 kHz, accounting for the 10% detection efficiency and 5 dB of losses, which include

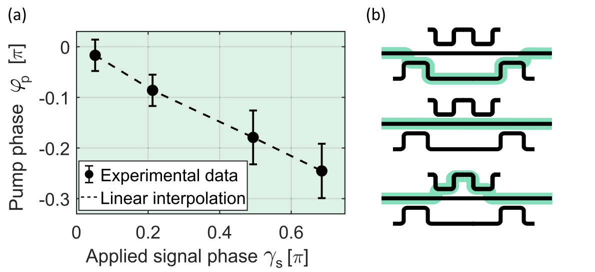

FIG. 3. (a) Experimental characterization of the correlation between a spurious pump phase contribution φ_p and an applied signal phase γ_s. The pump wavelength is 1561 nm. (b) Schematic of the phase manipulation stage qualitatively showing the contributions of the pump p_1 at the input of the second source. p_1 partially couples with the signal ADC (top), propagates along the central waveguide (middle), and couples with the pump ADC (bottom).

chip-to-fiber coupling losses, propagation losses, and off-chip filter losses. The idler and signal peak wavelengths are generated at 1291.6(5) and 1972(1) nm, respectively. After applying a known phase γ_s to the signal, we swept the pump phase γ_{p_1} to observe single-photon interference in the idler photon counts. In Fig. 4(a), we report two interference measurements, with $\gamma_s = 0$ and $\gamma_s = 0.21\pi$. The interference patterns are phase-shifted relative to each other, as the idler carries different phase information in the two measurements. Similarly to the measurements shown in Fig. 4(a), we

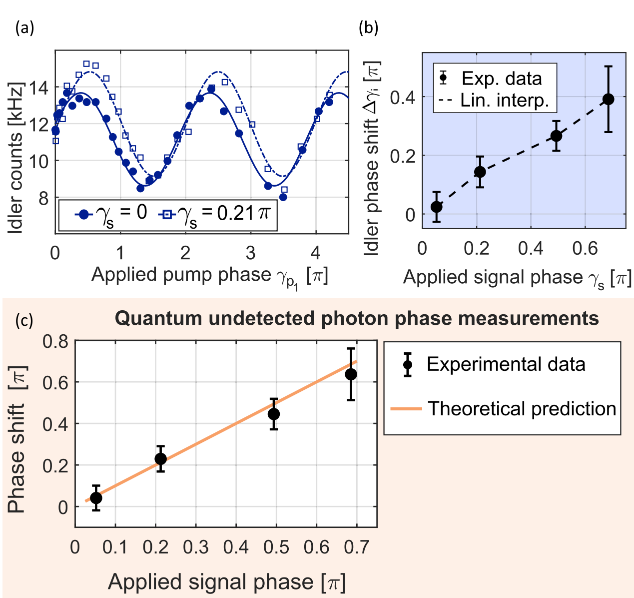

FIG. 4. Experimental results. (a) Idler counts as a function of γ_{p_1} for $\gamma_s = 0$ and $\gamma_s = 0.21\pi$. The dots represent the experimental data after the subtraction of the dark counts (325 Hz). The integration time per point is 1 s. The marker size is larger than the error bar. The lines represent the sinusoidal fit. The fitting function is of the form $Counts = a \times \sin(b\gamma_{p_1} + c) + d$, with a, b, c, and d the parameters of the fit. (b) Idler phase shift $\Delta\gamma_i$ as a function of γ_s. (c) Correspondence between the experimental data (dots) and the theoretical prediction (line).

acquired interferograms for four different values of γ_s. Each interference pattern was compared with a reference measurement taken with $\gamma_s = 0$. We call $\Delta\gamma_i$ the phase shift experienced by the idler interferogram when $\gamma_s \neq 0$. The experimental values for $\Delta\gamma_i$ are reported in Fig. 4(b), as a function of γ_s. The measured $\Delta\gamma_i$ has to be corrected by the phase shift φ_p experienced by the pump when applying the signal phase, as characterized in Fig. 3(a). The signal phase can be recovered, without detecting the signal photons, by looking at the phase shift $\gamma_{\mathrm{UP}} = \Delta\gamma_i - \varphi_p$. Indeed, we experimentally found a one-to-one correspondence, shown in Fig. 4(c), between the global measured phase shift γ_{UP} and the phase applied to the signal photons γ_s, meaning that we are actually sensing the phase probed by photons that are not detected.

In conclusion, we reported, to the best of our knowledge, the first UP experiment on a photonic chip. We developed a UP circuit on a silicon PIC that we used to retrieve the phase probed by the signal photons without detecting them. Our circuit is based on a novel spatial-mode SU(1,1) interferometer, where intermodal SFWM is used to generate highly non-degenerate photon pairs, with the idler in the O-band and the signal wavelength approaching 2 μm. Transverse waveguide-mode multiplexing is used to individually address the pump and signal phases. By pushing the non-degeneracy of the sources, we expect to place the probing photon at specific MIR wavelengths, suitable for practical sensing applications, paving the way for portable, low-cost, and mass-produced PIC based devices.

The supplementary material includes the full fringes in the idler counts for the four data points in Figs. 4(b) and 4(c).

The authors acknowledge financial support from the Spanish Ministry of Economy and Competitiveness through the project MAGICAL (PID2022-137952NB-I00, funded by MCIN/AEI/10.13039/501100011033/FEDER, UE). This project also received funding from the European Union's Horizon 2020 research and innovation program under the Marie Skłodowska-Curie Grant Agreement No. 956419. This work was partially funded by CEX2019-000910-S (MCIN/AEI/10.13039/501100011033), Fundació Cellex, Fundació Mir-Puig, and Generalitat de Catalunya through CERCA.

C.M. thanks Davide Rizzotti for his technical support.

AUTHOR DECLARATIONS

Conflict of Interest

The authors have no conflicts to disclose.

Author Contributions

Chiara Michelini: Data curation (equal); Formal analysis (equal); Investigation (equal); Validation (equal); Visualization (equal); Writing – original draft (equal); Writing – review & editing (equal). **Stefano Signorini**: Conceptualization (equal); Data curation (equal); Formal analysis (equal); Funding acquisition (equal); Investigation (equal); Methodology (equal); Validation (equal); Visualization (supporting); Writing – original draft (equal); Writing – review & editing (equal). **Lorenzo Pavesi**: Funding acquisition (equal); Resources (equal); Supervision (equal); Writing – review

& editing (equal). **Valerio Pruneri**: Funding acquisition (equal); Resources (equal); Supervision (equal); Writing – review & editing (supporting).

DATA AVAILABILITY

The data that support the findings of this study are available from the corresponding author upon reasonable request.

APPENDIX A: IDLER DETECTION PROBABILITY

Equation (1) is derived by adapting the calculation for an UP setup in the configuration of a low-gain SU(1,1) interferometer to the SFWM case, in the specific scenario in which the pumps, idler, and signal are not subjected to losses. In fact, it is well known that losses do not affect the phase information in an UP measurement,[10] but they only affect the visibility of the interference pattern. In the following, we report the main calculation to derive Eq. (1). We consider the case in which the multi-photon pair generation probability is negligible, and we will indicate as $|j\rangle_n$ ($j = s, i$) the Fock state $|1\rangle_j$ for photons generated in the nth source.

When the idler–signal pair is generated in the first source, it acquires a global phase $\gamma_i + \gamma_s$, and it is described by the state

$$|\psi\rangle_1 = e^{i(\gamma_i+\gamma_s)}|s\rangle_1|i\rangle_1. \tag{A1}$$

Alternatively, the pair is generated in the second source and carries the pumps' phase $\gamma_{p_0} + \gamma_{p_1}$,

$$|\psi\rangle_2 = e^{i(\gamma_{p_0}+\gamma_{p_1})}|s\rangle_2|i\rangle_2. \tag{A2}$$

By superposing the paths of the photons, and considering indistinguishability such that $|s\rangle_1 \equiv |s\rangle_2$ and $|i\rangle_1 \equiv |i\rangle_2$, the which-source information is erased, and the final state is

$$|\psi\rangle = \frac{1}{2}\left(e^{i(\gamma_{p_0}+\gamma_{p_1})} + e^{i(\gamma_i+\gamma_s)}\right)|s\rangle|i\rangle, \tag{A3}$$

where the 1/2 factor comes from normalization. The probability of detecting the idler is obtained by calculating the density matrix $|\psi\rangle\langle\psi|$, tracing out the signal state, and squaring the modulus of the probability amplitude for the idler state $|i\rangle$. The result is

$$P_i = \frac{1}{2}\left[1 + \cos\left(\gamma_{p_0} + \gamma_{p_1} - \gamma_i - \gamma_s\right)\right], \tag{A4}$$

which equals Eq. (1).

APPENDIX B: RELEVANT DESIGN PARAMETERS OF THE INTEGRATED CIRCUIT

In our design, the signal and the pump in the TE1 optical mode are selectively separated. The separation of these modes relies on both the transverse waveguide-mode and the spectral degrees of freedom, using ADCs specifically designed for each beam. Table I lists the dimensions of the waveguides' cross section, together with the length of the photon pair source (multimode waveguide) and the ADC's coupling length. We estimated the efficiency of our ADCs (full-3D FDTD simulation) to be greater than 95% for both ADCs operating in their designed spectral regions. However, the ADCs exhibit an efficiency greater than zero outside their intended spectral ranges: the signal ADC couples the pump p_1 with an efficiency of 10% and the pump ADC couples the signal with an efficiency of 20%.

The phase shifters are tungsten electrical resistors placed 1 μm above the corresponding waveguide. The geometry of the resistors is listed in Table II.

TABLE I. Design specifics. The width and the height refer to the cross section dimensions of the core of a channel waveguide, while the length corresponds to the dimension along the modes' propagation direction. For the ADCs, phase matching is met between the mode propagating in the single-mode waveguide and the first excited optical mode in the multimode waveguide. SM: single-mode waveguide. MM: multimode waveguide.

	Width SM	Width MM	Height	Length
Source	⋯	2 μm	0.22 μm	7.5 mm[a]
ADC (pump)	0.45 μm	0.935 μm	0.22 μm	28.6 μm[b]
ADC (signal)	0.8 μm	1.85 μm	0.22 μm	58.3 μm[b]

[a]Length of a single photon-pair source.
[b]Coupling length for a coupling distance of 0.2 μm.

TABLE II. Geometry of the phase shifters. The length, height, and width of the resistors are defined consistently with the corresponding dimensions of the waveguides on the chip.

	Width	Height	Length
Pump p_1	0.6 μm	0.3 μm	204.0 μm
Pump p_0 and idler	0.6 μm	0.3 μm	204.0 μm
Signal	0.6 μm	0.3 μm	534.8 μm

REFERENCES

[1] J. K. S. Poon, A. Govdeli, A. Sharma, X. Mu, F.-D. Chen, T. Xue, and T. Liu, "Silicon photonics for the visible and near-infrared spectrum," Adv. Opt. Photonics **16**, 1–59 (2024).

[2] M. P. Edgar, G. M. Gibson, R. W. Bowman, B. Sun, N. Radwell, K. J. Mitchell, S. S. Welsh, and M. J. Padgett, "Simultaneous real-time visible and infrared video with single-pixel detectors," Sci. Rep. **5**, 10669 (2015).

[3] O. Kahl, S. Ferrari, V. Kovalyuk, G. N. Goltsman, A. Korneev, and W. H. P. Pernice, "Waveguide integrated superconducting single-photon detectors with high internal quantum efficiency at telecom wavelengths," Sci. Rep. **5**, 10941 (2015).

[4] Y. Zhao, S. Kusama, Y. Furutani, W.-H. Huang, C.-W. Luo, and T. Fuji, "High-speed scanless entire bandwidth mid-infrared chemical imaging," Nat. Commun. **14**, 3929 (2023).

[5] D. Popa and F. Udrea, "Towards integrated mid-infrared gas sensors," Sensors **19**, 2076 (2019).

[6] Y. Ozaki, "Infrared spectroscopy—Mid-infrared, near-infrared, and far-infrared/terahertz spectroscopy," Anal. Sci. **37**, 1193–1212 (2021).

[7] I. E. Gordon, L. S. Rothman, C. Hill, R. V. Kochanov, Y. Tan, P. F. Bernath, M. Birk, V. Boudon, A. Campargue, K. V. Chance *et al.*, "The HITRAN2016 molecular spectroscopic database," J. Quant. Spectrosc. Radiat. Transfer **203**, 3–69 (2017).

[8] B. Fu, C. Zhang, W. Lyu, J. Sun, C. Shang, Y. Cheng, and L. Xu, "Recent progress on laser absorption spectroscopy for determination of gaseous chemical species," Appl. Spectrosc. Rev. **57**, 112–152 (2020).

[9] A. Rogalski, *Infrared Detectors* (CRC Press, 2010).

[10]G. Barreto Lemos, M. Lahiri, S. Ramelow, R. Lapkiewicz, and W. N. Plick, "Quantum imaging and metrology with undetected photons: Tutorial," J. Opt. Soc. Am. B **39**, 2200–2228 (2022).
[11]M. V. Chekhova and Z. Y. Ou, "Nonlinear interferometers in quantum optics," Adv. Opt. Photonics **8**, 104 (2016).
[12]Z. Y. Ou and X. Li, "Quantum SU(1,1) interferometers: Basic principles and applications," APL Photonics **5**, 080902 (2020).
[13]I. Kviatkovsky, H. M. Chrzanowski, E. G. Avery, H. Bartolomaeus, and S. Ramelow, "Microscopy with undetected photons in the mid-infrared," Sci. Adv. **6**, eabd0264 (2020).
[14]I. Kviatkovsky, H. M. Chrzanowski, and S. Ramelow, "Mid-infrared microscopy via position correlations of undetected photons," Opt. Express **30**, 5916–5925 (2022).
[15]D. A. Kalashnikov, A. V. Paterova, S. P. Kulik, and L. A. Krivitsky, "Infrared spectroscopy with visible light," Nat. Photonics **10**, 98–101 (2016).
[16]J. Dong, A. C. Cardoso, H. Zhou, J. Zhang, W. Nie, A. S. Clark, and J. G. Rarity, "Methane sensing via unbalanced nonlinear interferometry using a CMOS camera and undetected mid-infrared light," Appl. Phys. Lett. **126**, 061104 (2025).
[17]T. Ono, G. F. Sinclair, D. Bonneau, M. G. Thompson, J. C. F. Matthews, and J. G. Rarity, "Observation of nonlinear interference on a silicon photonic chip," Opt. Lett. **44**, 1277–1280 (2019).
[18]L.-T. Feng, M. Zhang, D. Liu, Y.-J. Cheng, G.-P. Guo, D.-X. Dai, G.-C. Guo, M. Krenn, and X.-F. Ren, "On-chip quantum interference between the origins of a multi-photon state," Optica **10**, 105–109 (2023).
[19]J. Frazer, T. Ono, and J. C. F. Matthews, "A Gigahertz configurable silicon photonic integrated circuit nonlinear interferometer," Quantum Sci. Technol. **10**, 025033 (2025).
[20]A. Hochrainer, M. Lahiri, M. Erhard, M. Krenn, and A. Zeilinger, "Quantum indistinguishability by path identity and with undetected photons," Rev. Mod. Phys. **94**, 025007 (2022).
[21]Y. Chen, J. Liu, Z. Yang, J. S. Wilkinson, and X. Zhou, "Optical biosensors based on refractometric sensing schemes: A review," Biosens. Bioelectron. **144**, 111693 (2019).
[22]S. Signorini, M. Mancinelli, M. Borghi, M. Bernard, M. Ghulinyan, G. Pucker, and L. Pavesi, "Intermodal four-wave mixing in silicon waveguides," Photonics Res. **6**, 805 (2018).
[23]S. Paesani, M. Borghi, S. Signorini, A. Maïnos, L. Pavesi, and A. Laing, "Near-ideal spontaneous photon sources in silicon quantum photonics," Nat. Commun. **11**, 2505 (2020).
[24]D. Dai and S. Wang, "Asymmetric directional couplers based on silicon nanophotonic waveguides and applications," Front. Optoelectron. **9**, 450–465 (2016).